

PIV measurements of the wake behind a rotationally oscillating circular cylinder

Sang-Joon Lee*, Jung-Yeop Lee

Department of Mechanical Engineering, Pohang University of Science and Technology, Pohang 790-784, Republic of Korea

Received 28 September 2006; accepted 22 June 2007

Available online 24 September 2007

Abstract

The near-wake behind a circular cylinder undergoing rotational oscillatory motion with a relatively high forcing frequency has been investigated experimentally. Experiments were carried out varying the ratio of the forcing frequency f_f to the natural vortex shedding frequency f_n in the range of 0.0 (stationary) to 1.6 at an oscillation amplitude of $\theta_A = 30^\circ$ and Reynolds number of $Re = 4.14 \times 10^3$. Depending on the frequency ratio ($F_R = f_f / f_n$), the near-wake flow could be divided into three regimes—non-lock-on ($F_R = 0.4$), transition ($F_R = 0.8, 1.6$) and lock-on ($F_R = 1.0$) regimes—with markedly different flow structures. When the frequency ratio was less than 1.0 ($F_R \leq 1.0$), the rotational oscillatory motion of the cylinder decreased the length of the vortex formation region and enhanced the mutual interaction between large-scale vortices across the wake centerline. The entrainment of ambient fluid seemed to play an important role in controlling the near-wake flow and shear-layer instability. In addition, strong vortex motion was observed throughout the near-wake region. The flow characteristics changed markedly beyond the lock-on flow regime ($F_R = 1.0$) due to the high frequency forcing. At $F_R = 1.6$, the high frequency forcing decreased the size of the large-scale vortices by suppressing the lateral extent of the wake. In addition, the interactions between the vortices shed from both sides of the cylinder were not so strong at this forcing frequency. As a consequence, the flow entrainment and momentum transfer into the wake center region were reduced. The turbulent kinetic energy was large in the region near the edge of the recirculation region, where the vortices shed from both sides of the cylinder cross the wake centerline for all frequency ratios except for the case of $F_R = 1.6$. The temporally resolved quantitative flow information extracted in the present work is useful for understanding the effects of open-loop active flow control on the near-wake flow structure. © 2007 Elsevier Ltd. All rights reserved.

Keywords: Rotational oscillation; Forcing frequency; Cylinder wake; Dynamic PIV; Flow control; Shear-layer instability; Fluid entrainment

1. Introduction

The wake behind a circular cylinder has been a major research topic for many years due to the simple geometry and interesting flow characteristics of this system. Williamson (1996) reviewed works on the vortex dynamics in the two-dimensional wake behind a circular cylinder, and more recently, Williamson and Govardhan (2004) summarized what is known about vortex formation behind stationary and oscillating cylinders. When vortices are shed from the upper and

*Corresponding author. Tel.: +82 54 279 2169.

E-mail address: sjlee@postech.ac.kr (S.-J. Lee).

lower sides of a cylinder, the flow pattern is maintained for some distance downstream. Due to the capacity of circular cylinders to shed large-scale vortices, the cylinder wake has many practical engineering and scientific applications.

Several active flow control techniques have been used to control the flow behind a circular cylinder. A representative active flow control technique is to apply a rotational oscillatory motion to the circular cylinder. In this technique, the interaction between the rotationally oscillating body and the surrounding fluid modifies the near-wake structure significantly by accelerating and decelerating the fluid around the cylinder according to the direction of rotation (Baek and Sung, 1998). When the adjacent fluid is accelerated by the cylinder rotation, flow separation is delayed or suppressed and the large-scale vortices formed previously are pushed downstream. In contrast, when the adjacent fluid is decelerated, the separated shear layer starts to roll up and large-scale vortices are formed. Therefore, the near-wake flow and vortex structure can be controlled considerably by applying a rotational oscillatory motion to the cylinder.

In terms of the net effect of flow control, open-loop active flow control without auxiliary devices is preferred as an effective scheme. Therefore, it is important to investigate the role of rotary oscillation with open-loop control on the near-wake flow characteristics with varying the forcing condition.

Rotational oscillatory motion can be easily applied and manipulated using simple electrical and mechanical devices. Although this type of flow control is a promising and effective method, it has been investigated in only a limited number of studies. For instance, Tokumaru and Dimotakis (1991) investigated the wake behind a rotationally oscillating cylinder at the high Reynolds number of $Re = 15000$. They found that the wake has four distinct flow modes depending on the forcing condition, and that the drag is reduced by about 80% at high forcing frequency. Taneda (1978) visualized the periodic shedding of vortices behind a rotationally oscillating cylinder for Reynolds numbers in the range $30 \leq Re \leq 300$ and Strouhal numbers of $0 \leq St_f (= f_f D / U_o) \leq 55$. The dead water region behind a cylinder disappeared at high forcing frequency. Filler et al. (1991) observed large velocity fluctuations and high response peaks at frequencies near the Karman frequency of the test cylinder. Moreover, they observed a phase difference of approximately 180° between the cylinder motion and the vortex shedding when the forcing frequency crossed the natural Karman frequency. Recently, Lee and Lee (2006) used hot-wire anemometry to investigate the modification of the near-wake behind a rotationally oscillating cylinder. They classified the wake patterns into five flow regimes and showed that the vortex shedding frequency was notably different in each flow regime. In addition, through a detailed study of the lock-on flow regime, they identified the threshold amplitude of oscillation (θ_i) at which the lock-on phenomenon occurs only at $F_R = 1.0$.

In a numerical study of the wake behind a rotationally oscillating cylinder, Baek and Sung (1998) investigated the temporal variation of vortex formation with varying oscillation frequency ($0.110 \leq S_f \leq 0.220$) and angular amplitude ($\theta_{max} = 15^\circ, 30^\circ$ and 60°) at $Re = 110$. The vortex formation mode changed when the forcing frequency approached the natural shedding frequency and relevant phase change (π -change) occurred across the natural shedding frequency. Mahfouz and Badr (2000) found that the lock-on phenomenon occurred when the forcing frequency was close to the natural shedding frequency, and that the lock-on frequency range widened as the oscillation amplitude was increased. Shiels and Leonard (2001) observed that the drag was reduced as a result of separation delay due to the presence of multipole vorticity structures in the boundary layer around an oscillating cylinder, and that the rotational oscillation method for drag reduction was effective only at high Reynolds numbers ($Re \geq 3000$). Dennis et al. (2000) and Poncet (2004) investigated the temporal variation of the large-scale vortex structure behind a rotationally oscillating cylinder at moderate Reynolds numbers with varying forcing conditions. They found that the near-wake flow structure and aerodynamic forces acting on the cylinder were varied significantly depending on the forcing conditions, especially the forcing frequency and oscillation amplitude. In addition, the flow patterns were distinctly different according to the flow regime, and the mutual interaction between vortices was strong for large Reynolds numbers and oscillation amplitudes.

However, there have been few experimental studies on the variation of the flow structure behind a rotationally oscillating cylinder at high Reynolds numbers. The main objective of the present study was to investigate the flow structure of the near-wake behind a rotationally oscillating circular cylinder experimentally, in particular the effect on the vortex structure of varying the frequency ratio ($F_R = f_f / f_n$, where f_f and f_n are the forcing frequency and the natural vortex shedding frequency, respectively). To mimic the conditions encountered in practical applications, the experiments were carried out under high forcing frequencies at a relatively high Reynolds number. Although the variation of velocity profiles in the near-wake behind a rotationally oscillating cylinder was examined by Lee and Lee (2006) using a point wise measurement technique, information on the modification of the whole flow field in the near-wake is required to understand the flow characteristics in detail. Therefore, in the present work, the temporal evolution of vortex structure and the variation of mean flow characteristics were investigated using a dynamic particle image velocimetry (PIV) velocity field measurement system. The effect of the active flow control technique was evaluated by comparing the experimental results obtained using a rotationally oscillating cylinder with those obtained using a stationary cylinder.

2. Experimental apparatus and method

2.1. Wind tunnel and experimental model

Experiments were carried out in a closed-return type subsonic wind tunnel with a test-section of 0.72 m (width) \times 0.6 m (height) \times 6.75 m (length). The freestream turbulence intensity in the test-section was less than 0.08% at $U_o = 10$ m/s. This level of inflow turbulence intensity is sufficient to check the modification of the wake structure behind a bluff body (Gerrard, 1954). The experimental model was a piece of acrylic pipe of length $L = 400$ mm and outer diameter $D = 30$ mm. The freestream velocity was fixed at $U_o = 2$ m/s and the corresponding Reynolds number based on the cylinder diameter was 4140. Since the aspect ratio of the cylinder model was $L/D = 13.3$, it can be roughly considered as a two-dimensional model (Graham, 1969). An end-plate was attached to each end of the cylinder model to maintain two-dimensional flow in the wake by minimizing the effect of the boundary layer developing along the wind tunnel sidewall. The shape and size of the end-plate were determined based on the results of Stansby (1974).

A schematic diagram of the rotational oscillatory motion of the cylinder and the coordinate system used in this study is shown in Fig. 1(a). The cylinder model was placed horizontally in the central region of the wind tunnel test-section. When the ratio of frontal area of a test model to the wind tunnel cross-section is larger than about 6%, the flow around the model is changed due to the blockage effect (West and Apelt, 1982; Rae and Pope, 1984). In the present experiments, the blockage ratio of the test cylinder and end-plates was about 8%. To account for the blockage ratio and wall interference effects, the formulas suggested by Maskell (1963) were used to correct the velocity values.

In the present study, the natural vortex shedding frequency (f_n) was 15.14 Hz. The Strouhal number based on the vortex shedding frequency and corrected freestream velocity was $St_n (= f_n D / U_o) = 0.214$. To test at high frequency ratios ($F_R = f_f / f_n$) up to $F_R = 1.6$ (where f_f is the forcing frequency), we designed a device capable of rotary oscillation

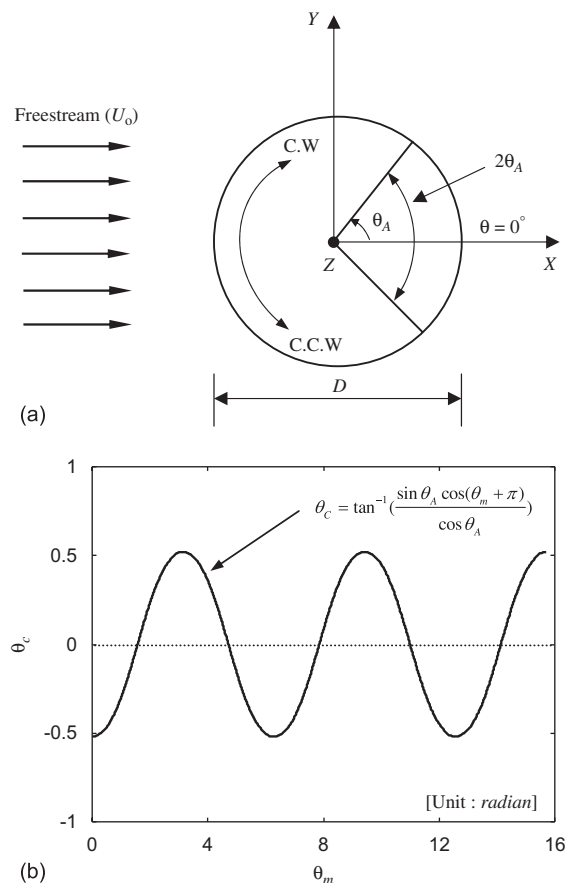


Fig. 1. (a) Schematic of the rotational oscillatory motion of a circular cylinder; (b) its waveform at $\theta_A = 30^\circ$ and coordinate system.

at frequencies higher than 25 Hz without angular velocity hysteresis. The device, which was driven by an AC servomotor, was placed outside the wind tunnel test-section to reduce interference with the oncoming flow, and was connected to the test cylinder using coupling elements. During the experiments, the oscillation amplitude was fixed at $\theta_A = 30^\circ$. The oscillatory motion of the cylinder and rotating motion of the driving motor can be represented as follows:

$$\theta_c = \tan^{-1} \left(\frac{\sin \theta_A \cos(\theta_m + \pi)}{\cos \theta_A} \right), \quad (1)$$

$$\theta_m(t) = 2\pi f_f t, \quad (2)$$

where θ_c is the phase angle of the cylinder oscillation ($-\theta_A \leq \theta_c \leq \theta_A$), θ_m is the phase angle of the motor rotation ($0 \leq \theta_m \leq 2\pi$), θ_A is the angular amplitude of the rotational oscillation, and t is time. The trigonometric waveform of the rotational oscillatory motion of the cylinder (Eq. (1)) is shown in Fig. 1(b).

2.2. Dynamic PIV system

In this study, a dynamic PIV system was used to investigate the modification of the near-wake flow structure. The dynamic PIV system overcomes some of the shortcomings of a convectional PIV system, with which the temporal evolution of flow structures is difficult to analyze due to its low frame rate (Bi et al., 2003). Fig. 2 shows a schematic diagram of the experimental set-up and measurement plane. The dynamic PIV system consists of a high-repetition pulse laser, a high-speed CMOS camera and a delay generator. The Nd:YLF laser (*Pegasus*) produces laser pulses with a wavelength of 527 nm and light intensity of 10 mJ at 2 kHz. The high-speed CMOS camera (*FASTCAM-Ultra APX*) has a $1K \times 1K$ pixel resolution at 2000 fps and a maximum frame rate of 10^5 fps. The high-speed camera was synchronized with the high-repetition laser using a precise delay generator. The timing diagram for synchronizing image capture by the high-speed camera and firing of the high-repetition laser is shown in Fig. 3(a).

Dynamic PIV measurements were performed for five frequency ratios ($F_R = 0.0, 0.4, 0.8, 1.0$ and 1.6) to examine the effect of forcing frequency on the near-wake flow structure. Particle images were captured at 1000 fps and each pair of particle images had a short time interval ($\Delta t = 150 \mu s$). From the captured particle images, instantaneous velocity fields were obtained using a cross-correlation PIV algorithm. The interrogation window size was 32×32 pixels and adjacent windows were 50% overlapped. The cylinder wake was illuminated with a 2-mm-thick laser sheet and the field of view was about $7 \times 7 \text{ cm}^2$. Olive oil particles with a mean diameter of 2–3 μm were seeded as tracer particles. A total of 1024 successive instantaneous velocity fields were obtained under each set of experimental conditions. They were ensemble averaged to obtain the spatial distributions of mean velocity, vorticity and turbulence statistics.

In this study, a flow visualization experiment was also performed under the same experimental conditions. Fig. 3(b) shows the timing diagram for this experiment. When the laser light sheet was illuminated many times in one exposed frame, the laser sheet looked like a continuous one. Since each illumination of the light sheet has a duration time of 180 ns, superimposed streaks of frozen flow structure were obtained successively.

3. Results and discussion

When rotational oscillatory motion is applied to a cylinder, the near-wake flow structure is dominated by the Reynolds number (Re), oscillation amplitude (θ_A) and frequency ratio (F_R). In addition, as previously mentioned by Mahfouz and Badr (2000) and Choi et al. (2002), the near-wake behind a rotationally oscillating cylinder exhibits mainly two distinct flow regimes, lock-on and non-lock-on, depending on forcing conditions. Here, the non-lock-on regime indicates the flow in which the periodic vortex shedding occurs at the natural vortex shedding (f_n), irrespective of the forcing frequency (f_f). In the present study, the frequency ratio was varied up to $F_R = 1.6$ ($f_f \approx 24 \text{ Hz}$) at a fixed Reynolds number (Re = 4140) and oscillation amplitude ($\theta_A = 30^\circ$). This range of frequency ratio encompasses both the lock-on and non-lock-on flow regimes. Under some forcing conditions, transitional characteristics are also observed in the near-wake when the forcing frequency is in the vicinity of the natural vortex shedding frequency.

3.1. Spectral analysis

Since the dynamic PIV technique acquires velocity fields at a high frame rate, the obtained flow information can also be used to conduct a spectral analysis of the type that in the past has usually been done using hot-wire anemometry and laser Doppler velocimetry (LDV). The power spectral density (PSD) distributions of the streamwise velocity component (U) extracted from the successive PIV results at the downstream location of $X/D = 2$, $Y/D = 0.5$ were obtained.

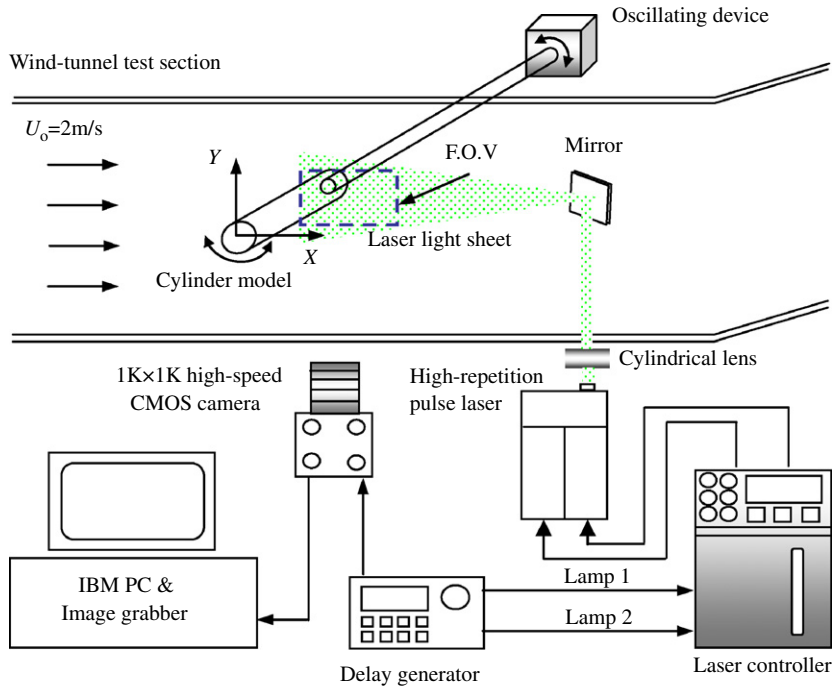


Fig. 2. Schematic diagram of experimental apparatus and measurement plane.

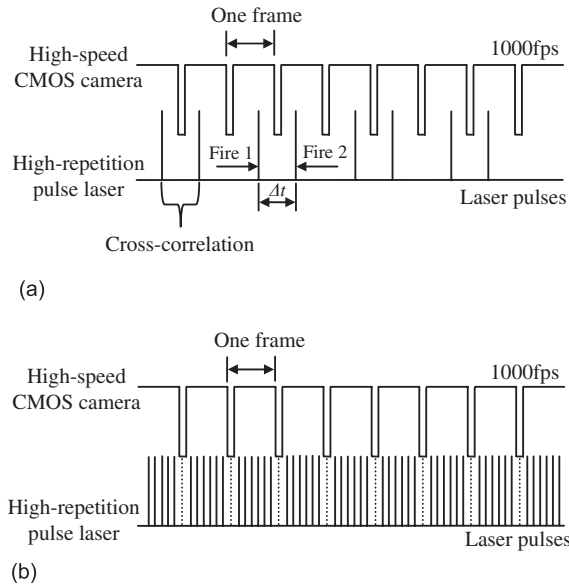


Fig. 3. Timing diagram for synchronizing a high-speed camera and a high-repetition laser: (a) dynamic PIV, (b) flow visualization.

In this experiment, instantaneous velocity fields were acquired consecutively at a sampling rate of 500 samples/s. This sampling rate is sufficient to obtain velocity signals for spectral analysis of the wake behind the oscillating cylinder. Due to periodic vortex shedding from the test cylinder, as shown in Fig. 4, each PSD distribution shows clear dominant peaks. Changes in the frequency ratio, F_R , which has a marked effect on the vortex shedding characteristics, may lead to variations in the flow structure of the near-wake behind the test cylinder. In these PSD distributions, $S(f)$ denotes the nondimensional streamwise velocity fluctuation (u/U_0) at the corresponding frequency.

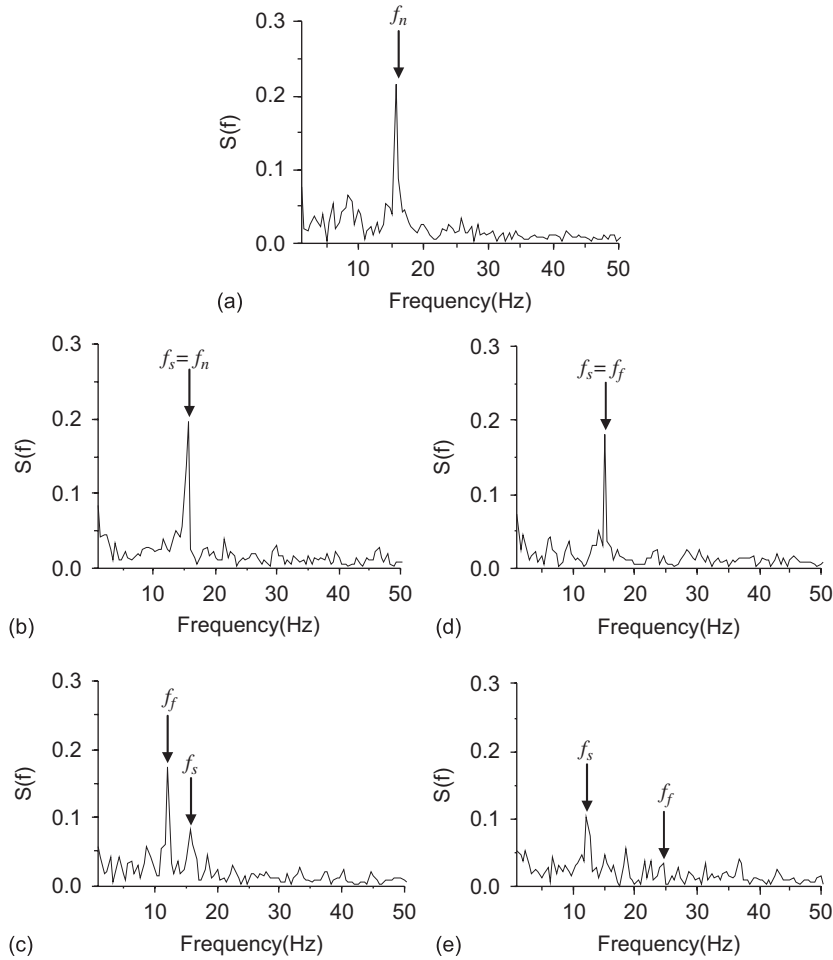


Fig. 4. Variation of PSD distribution of the streamwise velocity component (U) extracted at the downstream location $X/D = 2$, $Y/D = 0.5$. (a) $F_R = 0.0$, (b) $F_R = 0.4$, (c) $F_R = 0.8$, (d) $F_R = 1.0$ and (e) $F_R = 1.6$; f_n : natural vortex shedding frequency, f_f : forcing frequency, f_s : vortex shedding frequency.

For the stationary cylinder ($F_R = 0.0$, Fig. 4(a)), a single peak is observed at the natural vortex shedding frequency (f_n) due to the dominant vortex structure. The Strouhal number St_n based on the natural vortex shedding frequency and the blockage-corrected freestream velocity is 0.214. This value is within the Strouhal number range reported for the shear-layer transition regime at the corresponding Reynolds number [$Re = 4140$; Zdravkovich (1997)]. At $F_R = 0.4$ (Fig. 4(b)), even though the cylinder is undergoing oscillatory motion, the PSD distribution shows vortex shedding characteristics the same as those observed for the stationary cylinder. Therefore, this regime can be classified as the low-frequency non-lock-on regime. This non-lock-on regime is usually observed when the difference between the forcing frequency (f_f) and the natural vortex shedding frequency (f_n) is large (Mahfouz and Badr, 2000).

For the case of $F_R = 0.8$ (Fig. 4(c)), two dominant peaks appear at the forcing frequency and vortex shedding frequency (f_s) near the natural frequency, respectively. In this flow regime, the combined effect of f_f and f_s is observed in the PSD distribution. This regime can therefore be classified as a low-frequency transition regime. As the forcing frequency is increased up to a certain frequency between the non-lock-on and lock-on regimes, the flow structure switches back and forth between the two regimes intermittently. Similarly, Mahfouz and Badr (2000) also observed two intermittent vortex shedding frequencies in a numerical study of the flow around a rotationally oscillating cylinder. As the forcing frequency approaches the natural vortex shedding frequency, the dominant vortex shedding is exactly synchronized with the rotational oscillatory motion of the cylinder due to the enhanced mutual interaction between them. In this lock-on regime ($F_R = 1.0$), vortices are shed at the same frequency as the forcing frequency ($f_s = f_f$), resulting in a PSD distribution consisting of a single dominant peak at the imposed forcing frequency, as shown in Fig. 4(d).

On further increase of the forcing frequency to $F_R = 1.6$ (Fig. 4(e)), two distinct peaks are once again observed in the PSD distribution. The first peak appears at the vortex shedding frequency, which is lower than the natural frequency. The rather weak but still clear second peak is observed at the imposed forcing frequency, and can be regarded as a dominant peak since the forcing frequency is an input parameter in the present flow control method. The frequency ratio $F_R = 1.6$ therefore seems to correspond to a high-frequency transition regime. The presence of two peaks in the PSD distribution indicates intermittent vortex shedding in the wake, a flow characteristic that may significantly affect the near-wake structure. In addition, the vortex shedding frequency f_s and forcing frequency f_f have a relationship of $f_s \approx f_f/2$, which seems to be closely related to the variation of the lift coefficient in the transition regime observed by Mahfouz and Badr (2000). On the other hand, the ratio $f_s \approx f_f/2$ seems to result from the intermittent change of vortex shedding between regular and irregular modes (see discussion of Fig. 7 below), rather than from lock-on by the sub-harmonic of f_f . However, at $F_R = 1.6$, f_s is smaller than the natural shedding frequency f_n , since f_f is smaller than $2f_n$ ($f_f < 2f_n$). Moreover, since the vortex shedding is unstable due to the higher forcing frequency, and the vortex shedding displays intermittency involving two modes, the amplitude of PSD at the forcing frequency is decreased. This may be due to a deviation from the lock-on regime whereby the oscillatory motion of the cylinder and the vortex shedding are not synchronized, as mentioned by Lee and Lee (2006). They described the detailed frequency characteristics in the transition regime and the variation of the PSD distribution with respect to the frequency ratio. The relatively small amplitude at higher forcing frequency is well matched with the results of Filler et al. (1991), as shown in their typical frequency response curve.

Examination of the PSD distributions of the streamwise velocity component (U) extracted at the downstream location $X/D = 2$, $Y/D = 0.5$ for frequency ratios of $F_R = 0.0$ – 1.6 (Fig. 4) shows that each flow regime has significantly different flow characteristics. The PSD results and identification of flow regime are well matched with the results of Lee and Lee (2006), in which the PSD analysis was carried out using hot-wire anemometry under the same experimental conditions. From this, we can see that the temporally resolved dynamic PIV data can be used to perform spectral analysis of wake flows.

3.2. Instantaneous flow fields

The temporal evolution of the instantaneous velocity field during the first half of the period ($0T \sim 0.5T$) is shown in Fig. 5. For the case of a stationary cylinder ($F_R = 0.0$), the starting point ($\Phi = 0T_n$) of the period is chosen to coincide with the moment at which the roll-up phenomenon begins to occur in the upper shear layer. For the cases with an oscillating cylinder ($F_R = 0.4$ and 1.0), the period begins when the cylinder starts to rotate in a clockwise direction.

The instantaneous velocity fields show significant changes in the flow structure as the frequency ratio F_R is varied. For the stationary cylinder ($F_R = 0.0$, Fig. 5(a)), the rolling-up vortex ($\Phi = 0T_n$) grows in the upper shear layer, and after the first half of the period ($\Phi = 0.5T_n$), the roll-up phenomenon occurs again in the lower shear layer with the saddle point marked ‘S’ in the figure. From the temporal evolution process for the stationary cylinder (Fig. 5(a)), we can clearly discern the downstream movement of the vortex core as the phase changes. For the case of $F_R = 0.4$ (Fig. 5(b)), however, although the vortex shedding occurs at the natural vortex shedding frequency, the near-wake structure is quite different from that of the stationary cylinder ($F_R = 0.0$). The time period is based on the vortex shedding frequency (f_s), because the vortex shedding occurs irrespective of the forcing frequency (f_f). At the starting phase $\Phi = 0T_s$, the roll-up phenomenon is observed in the upper shear layer and it develops into a large-scale vortex up to the phase $\Phi = 0.4T_s$. The roll-up process occurs closer to the cylinder compared with the flow around a stationary cylinder. A large amount of fluid is entrained into the near-wake region during this process as the rolled-up small-scale vortex grows into a large-scale vortex. In addition, after the first half of the period, the roll-up phenomenon and saddle point appear again in the lower shear layer, indicating the start of another vortex formation process during the second half of the period.

For $F_R = 1.0$ (Fig. 5(c)), the phases of the rotational oscillatory motion of the cylinder and vortex shedding phenomenon are exactly synchronized, confirming that this system is in the lock-on regime. In this lock-on regime, the roll-up phenomenon occurs in the region just behind the cylinder. In addition, a vortex develops into a large-scale vortex as the adjacent fluid is decelerated and shed during the acceleration process. As a result, a large-scale vortex exists in the upper part just behind the cylinder at $\Phi = 0T_f$. The developed large-scale vortex begins to shed when the cylinder starts to rotate in the clockwise direction. During the shedding process, another vortex is observed in the opposite side at $\Phi = 0.2T_f$ and develops into a large-scale one at $\Phi = 0.5T_f$. This vortex formation process is repeated in the same manner during each period, supporting the PSD results shown in Fig. 4(d).

Fig. 6 shows the visualized flow of the near-wake at $F_R = 0.8$. Two different vortex shedding modes can be seen: the regular shedding mode (Fig. 6(a)) due to the oscillatory motion of the cylinder; and the irregular shedding mode (Fig. 6(b)) due to the hysteresis-like-mismatch between the oscillatory motion of the cylinder and the natural vortex

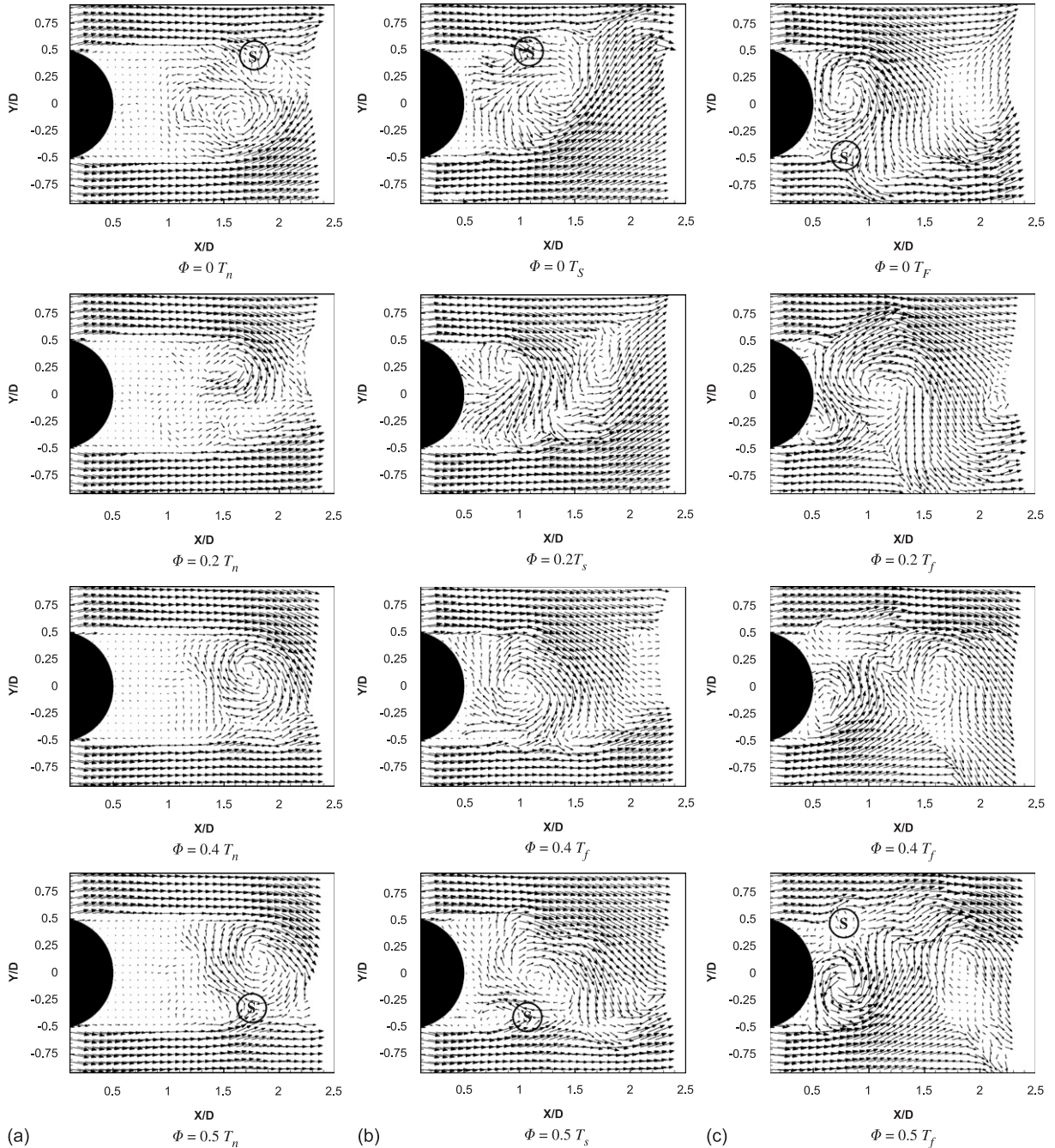


Fig. 5. Temporal evolution of vortex structure during the first half of the period ($0T-0.5T$) in the case of $Re = 4140$ and $\theta_A = 30^\circ$ at different frequency ratio: (a) $F_R = 0.0$, (b) $F_R = 0.4$ and (c) $F_R = 1.0$.

shedding motion. In the regular shedding mode, the roll-up phenomenon occurs at $X/D \approx 0.64$. Therefore, the vortex formation length is reduced, compared with that of the flow around the stationary cylinder. In the irregular shedding mode; however, the recirculation bubble-like wake pattern appears due to entrainment of a large amount of fluid, which occurs almost at the same time at both the upper and lower sides. This irregular shedding mode recovers to a regular vortex shedding configuration when the roll-up is stabilized and entrainment occurs alternately at only one side as in the

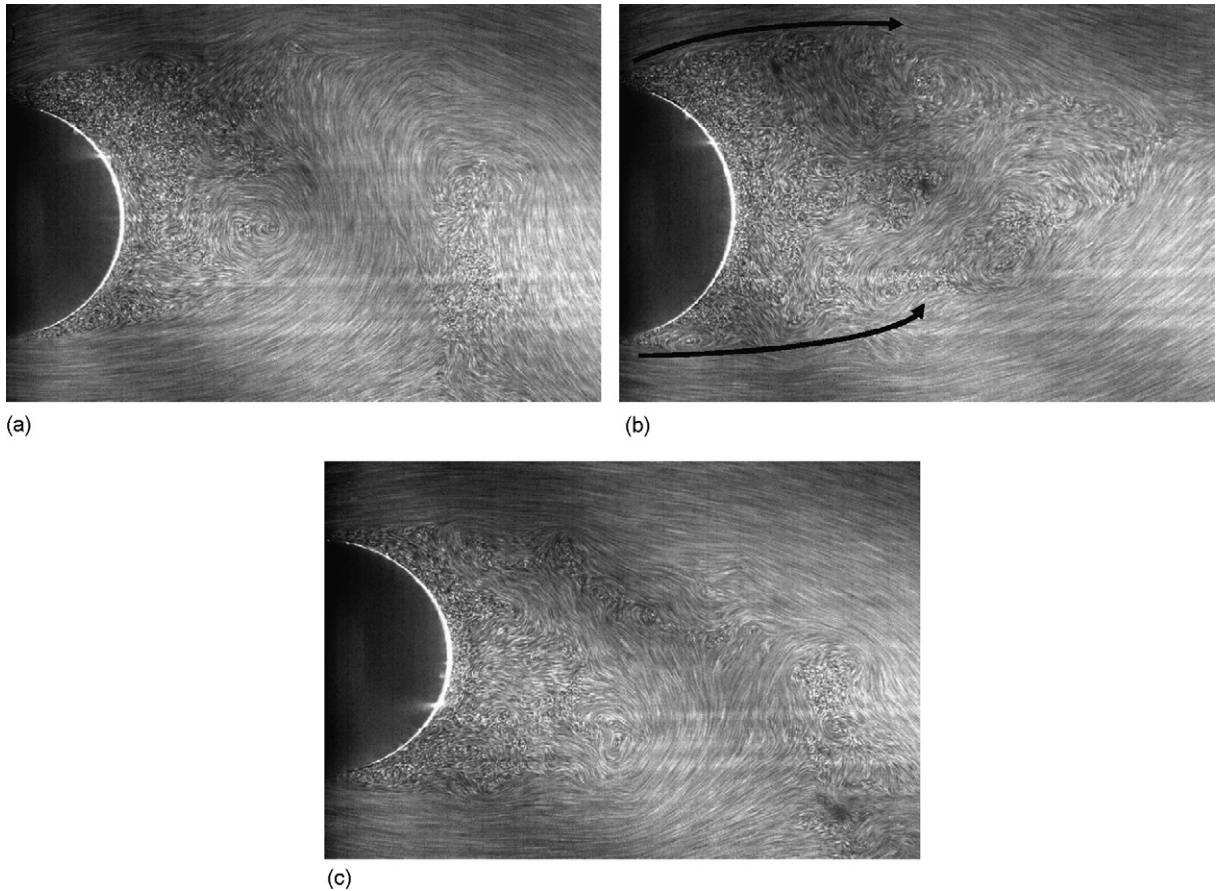


Fig. 6. Two vortex shedding modes in the transition regime and small-scale vortices at $F_R = 0.8$: (a) regular shedding mode, (b) irregular shedding mode and (c) small-scale vortices distributed along the shear layer.

regular shedding mode. Due to the presence of these two vortex shedding modes, two peaks appear in the corresponding PSD distribution of the low-frequency transition regime (Fig. 4(c)).

The flow structures shown in Figs. 5 and 6 are very similar to those visualized by Lee and Lee (2006). However, with the aid of temporally resolved flow information, we could observe the temporal evolution of the flow structure in greater detail. In particular, the switching of the vortex shedding mode in the transition regime and its hysteresis-like-mismatch mechanism are clearly observed in the present study.

As the frequency ratio F_R is increased, the length of the vortex formation region decreases, and the size of the shedding vortices increases. These changes occur because the acceleration and deceleration of the fluid adjacent to the cylinder surface is proportional to F_R . For the stationary cylinder ($F_R = 0.0$), the roll-up phenomenon occurs at the end of the shear layer, which is located at approximately $X/D = 1.51$. For the cases of $F_R = 0.4$ and 1.0 , however, the roll-up occurs at $X/D \approx 0.85$ and just behind the cylinder ($X/D \approx 0.52$), respectively. The variation of roll-up location is also well matched with the variation of the saddle point as a function of F_R in Fig. 5, since the saddle point appears as the roll-up occurs to form a new vortex (Gerrard, 1966). In addition, entrainment of a large amount of ambient fluid is observed in the near-wake region when the oscillating motion is applied to the cylinder. This may contribute to the drag reduction, because the recovery of the velocity deficit inside the wake and the momentum transfer into the wake region are proportional to the amount of fluid entrained from outside of the wake (Lee and Lee, 2006). In particular, Fig. 6(c) shows numerous small-scale vortices distributed along the shear layers, which resemble the topological vorticity pattern for which Shiels and Leonard (2001) observed the maximum drag reduction effect in the rotationally oscillating circular cylinder. This kind of near-wake flow pattern is occasionally observed in flows in which the vortex shedding mode changes intermittently. Lee and Lee (2006) reported that the drag reductions for the $F_R = 0.4$ and 0.8 systems are about 24.25% and 32.82%, respectively. From the results above, we can see that the near-wake flow structure is modified significantly and the shear-layer instability is greatly affected by the rotational oscillatory motion of the cylinder. These

findings support the assertion that the effect of the rotational oscillation on the shear-layer instability is the main flow control mechanism (Ongoren and Rockwell, 1988).

The visualized flow at $F_R = 1.6$ also shows transitional flow characteristics in the form of regular and irregular vortex shedding patterns, as shown in Figs. 7(a) and (b), respectively. The flow switches between the two shedding modes intermittently in the same manner as the $F_R = 0.8$ system. This intermittent variation in the vortex shedding pattern gives rise to the two peaks observed in the PSD distribution (Fig. 4(e)). The roll-up phenomenon and vortex development occur very rapidly at $F_R = 1.6$. In addition, the vortices are relatively small compared to those observed for the systems with $F_R \leq 1.0$. The high-frequency forcing seems to decrease the size of the vortices and suppress the lateral extent of the wake, as shown in Fig. 7(a). Moreover, the large-scale vortices shed from the top and bottom of the cylinder do not cross the wake centerline and move downstream without interacting with each other, decreasing the degree of fluid entrainment. Therefore, the momentum transfer into the wake center region is constrained, increasing the drag force acting on the cylinder. Lee and Lee (2006) found that the drag was increased about 72.16% at $F_R = 1.6$ and that flow separation was enhanced due to the high forcing frequency, which induces vortex coalescence by increasing the instability in the separated shear layer. The present results support the *forcing-induced enhancement of flow separation* mechanism reported by Lee and Lee (2006).

The vertical velocity (V/U_o) profiles extracted along the X -axis ($Y/D = 0$) from instantaneous velocity fields for all frequency ratios at $\Phi = 0T$ are shown in Fig. 8. For the cases of $F_R = 0.4, 0.8$ and 1.0 , the vertical velocity V/U_o reaches values up to $V/U_o \approx 1$ as a result of enhanced entrainment of ambient fluid across the wake centerline. At $F_R = 1.6$,

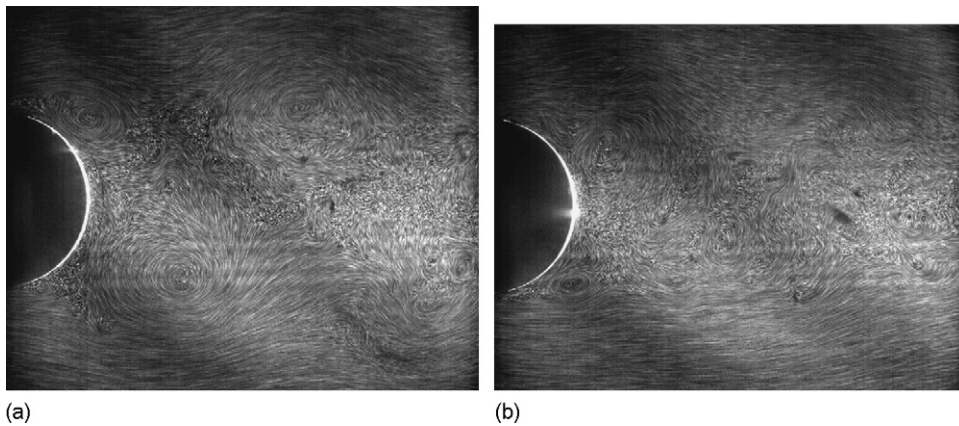


Fig. 7. Two vortex-shedding modes in the transition regime at $F_R = 1.6$: (a) regular shedding mode and (b) irregular shedding mode.

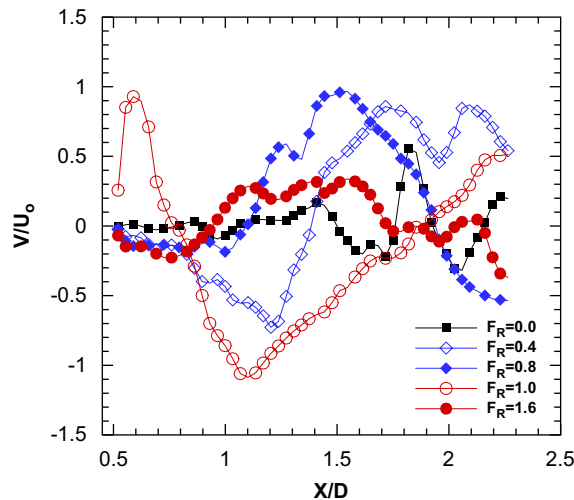


Fig. 8. Instantaneous vertical velocity profiles along the X -axis at $Y/D = 0$ and $\Phi = 0T$.

however, the vertical velocity V/U_o is less than 0.4, indicating decreased entrainment of ambient fluid across the wake centerline, as mentioned in the discussion of Fig. 7.

Fig. 9 shows the variation of the vortex center trajectories in the upper part of the wake along the Y -axis with respect to the frequency ratio F_R during the first half of the period ($0T \sim 0.5T$) of the regular vortex shedding mode. The vortex center trajectories were obtained by calculating streamlines from instantaneous velocity fields for each period. The actual locations of the vortex center along the downstream direction (X -axis) differ according to F_R , because the convection velocity of the large-scale vortices and the time interval of each period vary markedly depending on the frequency ratio F_R . However, the difference in the lateral motion of vortices is clearly observed in Fig. 9. For the stationary cylinder ($F_R = 0.0$), the vortex is formed at approximately $Y/D = 0.5$ and its center location approaches the wake centerline ($Y/D = 0$) gradually. At $F_R = 0.4$ and 0.8 , the vortex center moves toward the wake centerline and crosses the wake centerline at $\Phi = 0.4T$. For $F_R = 1.0$, the vortex center trajectory maintains its location around the wake centerline up to $\Phi = 0.4T$ and then starts to move upward at $\Phi = 0.5T$ due to the growth of the new vortex on the opposite side of the wake centerline. When $F_R \leq 1.0$, the vortex center location is arranged sequentially according to F_R at $\Phi = 0T$. In addition, the center locations of the vortices move toward the wake centerline due to enhanced mutual interaction and maintain their trajectory near the wake centerline. These vortex motions match well with the flow visualizations in Figs. 5 and 6. However, at $F_R = 1.6$, the vortex center remains at the same distance from the wake centerline beyond $Y/D = 0.3$ and does not approach the wake centerline as shown in Fig. 7(a). Among the frequency ratios tested in this study, the vortex center location for the case of $F_R = 1.6$ is the farthest from the wake centerline after $\Phi = 0.2T$, indicating weak entrainment across the wake centerline.

3.3. Mean flow fields

The spatial distributions of streamwise mean velocity, vorticity and turbulent kinetic energy (TKE) were obtained by ensemble averaging 1024 instantaneous velocity fields for each frequency ratio.

Fig. 10 shows contour plots of the streamwise mean velocity (U/U_o) distributions and streamlines in the XY plane measured at the mid-section of the cylinder. From this figure, we can see the behavior of large-scale vortices and the variation of the mean flow fields with changes in the frequency ratio. In addition, the recirculation regions enclosed by the shear layer can be observed. Near the middle of the recirculation region, where the streamlines converge, the streamwise mean velocity is lowest, with small negative values. Beyond this location, the streamwise mean velocity increases gradually.

For the stationary cylinder ($F_R = 0.0$), the recirculation region extends beyond the field of view chosen in this experiment. As the frequency ratio is increased, the length of the recirculation region decreases, since it is proportional to the distance from the location where the vortex is generated. For $F_R = 0.4, 0.8$ and 1.0 , the length of the recirculation region is approximately $X/D = 1.48, 1.24$ and 1.13 , respectively. This shortening of the recirculation region can be mainly attributed to the formation of the vortex in the region close to the cylinder occurring increasingly earlier as the frequency ratio is increased, because the

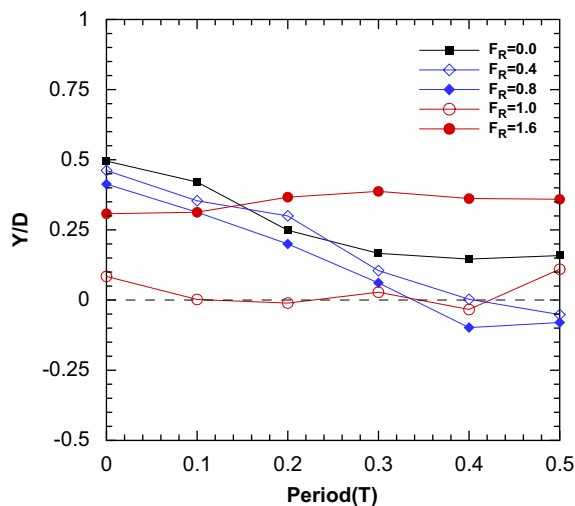


Fig. 9. Variation of vortex center trajectories in the upper part with respect to the frequency ratio F_R during the first half of the period ($0T \sim 0.5T$).

acceleration and deceleration of the fluid adjacent to the cylinder surface is proportional to the frequency ratio. In addition, the trend in the length of the recirculation region observed here is in good agreement with the variation in omnidirectional velocity fluctuations measured by Lee and Lee (2006) along the wake centerline as a function of frequency ratio. However, it is interesting to note that the length of the recirculation region is about $X/D = 1.61$ at $F_R = 1.6$, which is relatively long compared with the systems with lower frequency ratios. Taking into consideration the vortex trains noted above in the regular shedding mode (Fig. 7(a)) and irregular shedding mode (Fig. 7(b)), the occurrence of recirculation region shown in Fig. 10(e) seems to be due to the irregular vortex-shedding pattern and the behavior of vortices in the regular shedding mode.

Contour plots of the spanwise vorticity (w_z) in the longitudinal XY plane are shown in Fig. 11. Contours of positive and negative spanwise vorticity are depicted as solid and dashed lines, respectively. Both positive and negative values are distributed nearly symmetrically along the $Y/D = 0$ axis.

The spanwise vorticity w_z has large values at both sides of the cylinder along the separated shear layers and at the locations where the large-scale vortices are formed. Consistent with the results presented above, the leading head parts of the vorticity contours are contracted and have a more or less circular shape. In addition, the locations of the vortex centers shift back toward the cylinder as the frequency ratio is increased. Moreover, in the region just behind the

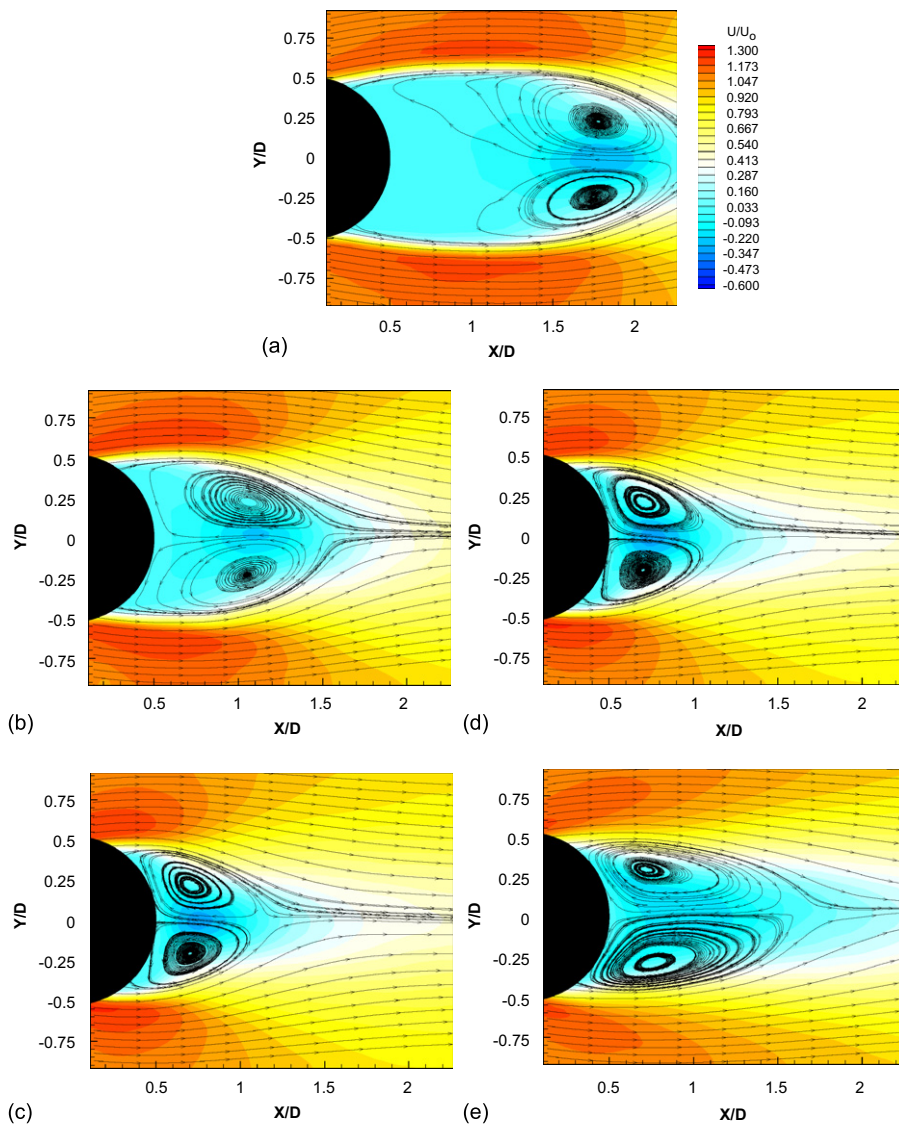


Fig. 10. Contour plots of streamwise mean velocity (U/U_0) and streamlines in the XY plane according to the frequency ratio F_R : (a) $F_R = 0.0$, (b) $F_R = 0.4$, (c) $F_R = 0.8$, (d) $F_R = 1.0$ and (e) $F_R = 1.6$.

cylinder surface, the vorticity gradually increases with increasing frequency ratio since the acceleration tangential to the cylinder surface is proportional to the frequency ratio. In particular, when the frequency ratio is increased to 1.0 and 1.6, the spanwise vorticity has distinctively larger values and its contours are elongated in the downstream direction, respectively.

Fig. 12 compares the ensemble-averaged TKE distributions measured in the mid-section of the longitudinal XY plane at various frequency ratios. All instantaneous velocity fields were statistically averaged to obtain spatial distributions of turbulent statistics.

The TKE k was calculated using the following two-dimensional approximation:

$$\bar{w}^2 \approx \frac{1}{2}(\bar{u}^2 + \bar{v}^2), \quad k = \frac{1}{2}\rho(\bar{u}^2 + \bar{v}^2 + \bar{w}^2) \approx \frac{3}{4}\rho(\bar{u}^2 + \bar{v}^2), \quad (3)$$

where u , v and w are the fluctuating velocity components of U , V and W , respectively. Due to the assumption of an isotropic turbulence structure, the real TKE will differ slightly from the present results in regions with non-isotropic turbulence structure.

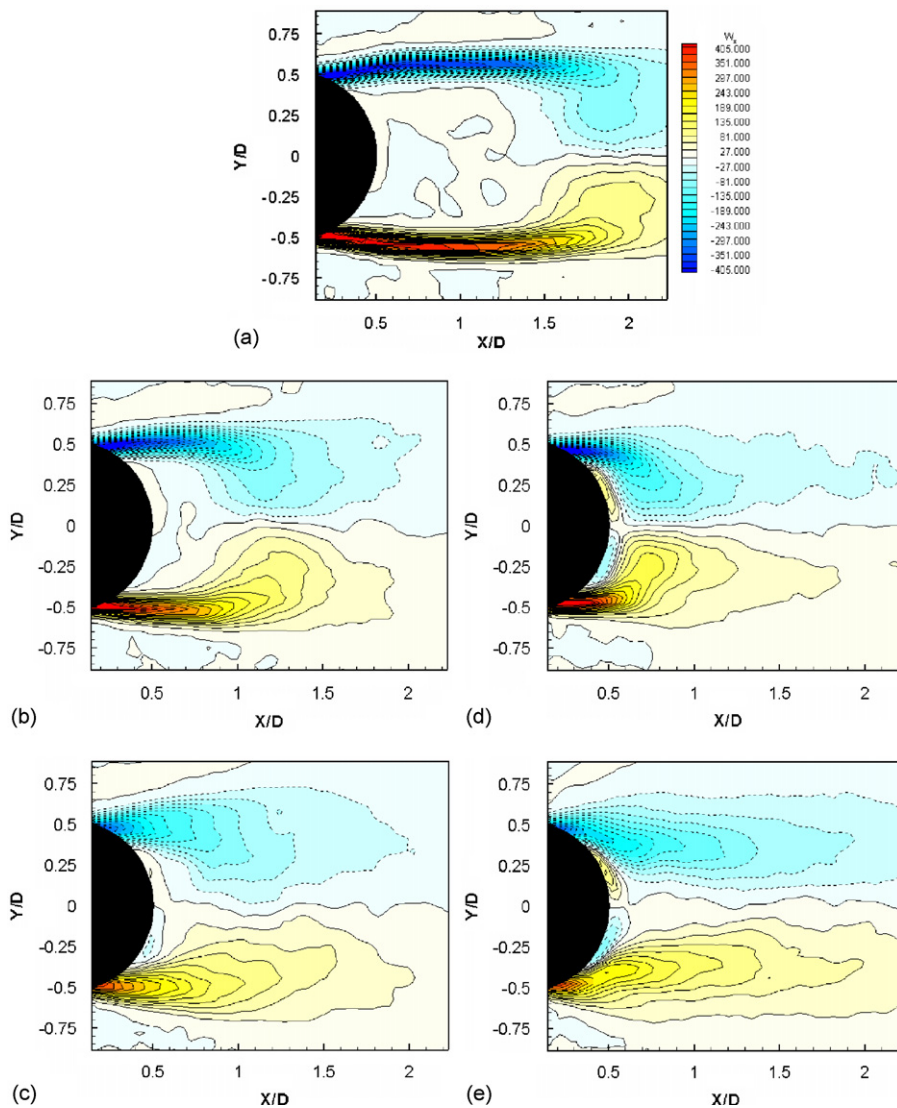


Fig. 11. Contour plots of spanwise vorticity (w_z) in the longitudinal XY plane with respect to the frequency ratio F_R : (a) $F_R = 0.0$, (b) $F_R = 0.4$, (c) $F_R = 0.8$, (d) $F_R = 1.0$ and (e) $F_R = 1.6$.

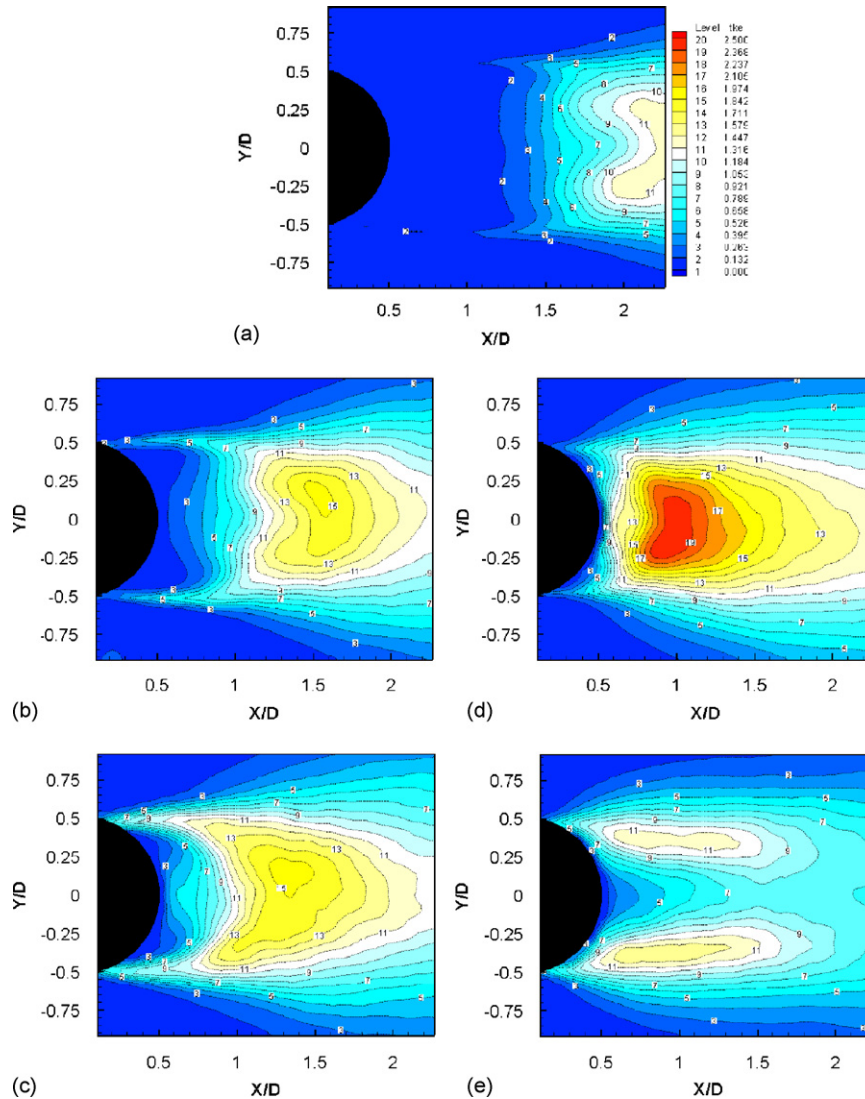


Fig. 12. Contour plots of turbulent kinetic energy (TKE) in the longitudinal XY plane according to the frequency ratio F_R : (a) $F_R = 0.0$, (b) $F_R = 0.4$, (c) $F_R = 0.8$, (d) $F_R = 1.0$ and (e) $F_R = 1.6$.

In the contour plots, the TKE has large values along the wake centerline ($Y/D = 0$) due to strong mutual interaction between vortices across the wake centerline. As the vortex formation region is shortened with increases in the frequency ratio, the contours also move toward the cylinder. Moreover, the maximum TKE value increases as the frequency ratio F_R is increased up to $F_R = 1.0$, and then decreases on further increase of F_R to 1.6. This indicates that the mutual interaction between vortices is strongest at $F_R = 1.0$, as shown in Fig. 5(c). For $F_R = 0.4, 0.8$ and 1.0 , the maximum TKE values are observed at $X/D = 1.58, 1.34$ and 1.0 on the $Y/D = 0$ axis, respectively. These locations are very near the edge of the recirculation region shown in Fig. 10.

The TKE contour plot for $F_R = 1.6$ shows quite a different configuration compared with the other cases. The TKE has large values in the regions above and below the wake centerline, and these zones of large TKE are distributed symmetrically about the centerline. This seems to be due to the behavior of the large-scale vortices in this system; specifically, the vortices do not show active motion across the wake centerline and shed downstream with a straight trajectory, as discussed in relation to Figs. 7 and 9. Therefore, these findings provide further confirmation that the mutual interaction of vortices across the wake centerline and fluid entrainment are weak at $F_R = 1.6$.

4. Conclusion

The flow characteristics of the near-wake behind a rotationally oscillating circular cylinder were investigated experimentally with varying the frequency ratio F_R . The velocity fields in the near-wake for each system were measured using a dynamic PIV technique.

The cylinder wake has different flow regimes, namely non-lock-on, transition and lock-on flow regimes, depending on the frequency ratio. For each flow regime, the consecutive instantaneous velocity fields show a different vortex formation process, which is well matched with the corresponding PSD distribution.

Since the acceleration and deceleration of flow tangential to the cylinder surface are proportional to the frequency ratio, the flow structure in the near-wake varies markedly with changes in the frequency ratio. Especially, the flow characteristics change substantially beyond the lock-on flow regime ($F_R = 1.0$). When the frequency ratio is smaller than 1.0 ($F_R \leq 1.0$), the length of the vortex formation region decreases as the forcing frequency is increased. The rotational oscillatory motion of the cylinder enhances the entrainment of ambient fluid into the near-wake region, resulting in strong mutual interaction between large-scale vortices. Moreover, the entrained fluids considerably influence shear-layer instability and the vortex formation process. From these results, we can see that the main flow control mechanism of the rotational oscillation is to control the shear-layer instability arising from the enhanced entrainment of ambient fluid. However, at the high frequency forcing of $F_R = 1.6$, the large-scale vortices develop very rapidly and the lateral extent of the wake is diminished; as a consequence, the vortices are smaller under this forcing condition than for $F_R \leq 1.0$. In addition, in the transition regimes ($F_R = 0.8$ and 1.6), the flow structure switches back and forth between the regular shedding mode and irregular shedding mode.

The variation of the mean flow fields as a function of frequency ratio is closely related to the behavior of the large-scale vortices. For $F_R = 0.4, 0.8$ and 1.0 , the edge of the recirculation region is located at approximately $X/D = 1.48, 1.24$ and 1.13 , respectively. The mutual interaction between vortices across the wake centerline is strongest in these edge regions. In the same manner, the TKE has maximum values near the edge, at $X/D = 1.58, 1.34$ and 1.0 , respectively. At $F_R = 1.6$, the configuration of the mean flow field distribution differed from that observed for the systems with $F_R \leq 1.0$, due to the suppression of the mutual interaction of large-scale vortices across the wake centerline and reduced entrainment of ambient fluid.

The rotational oscillatory motion of a circular cylinder was found to be an effective and promising method for controlling the near-wake flow structure. In addition, the present results show that temporally resolved quantitative and qualitative flow information is useful in understanding the cyclic variation of vortex structure and in analyzing the effect of open-loop active flow control on the near-wake flow structure.

Acknowledgment

This work was supported by the Korea Science and Engineering Foundation (KOSEF) through the National Research Lab. Program funded by the Ministry of Science and Technology (No. M10600000276-06J0000-27610).

References

- Baek, S.J., Sung, H.J., 1998. Numerical simulation of the flow behind a rotary oscillating circular cylinder. *Physics of Fluids* 10, 869–876.
- Bi, W., Sugii, Y., Okamoto, K., Madarame, H., 2003. Time-resolved proper orthogonal decomposition of the near-field flow of a round jet measured by dynamic particle image velocimetry. *Measurement Science and Technology* 14, L1.
- Choi, S.H., Choi, H.C., Kang, S.M., 2002. Characteristics of flow over a rotationally oscillating cylinder at low Reynolds number. *Physics of Fluids* 14, 2767–2777.
- Dennis, S.C.R., Nguyen, P., Kocabiyik, S., 2000. The flow induced by a rotationally oscillating and translating circular cylinder. *Journal of Fluid Mechanics* 407, 123–144.
- Filler, J.R., Marston, P.L., Mih, W.C., 1991. Response of the shear layers separating from a circular cylinder to small-amplitude rotational oscillations. *Journal of Fluid Mechanics* 231, 481–499.
- Gerrard, J.H., 1954. A disturbance-sensitive Reynolds number range of the flow past a circular cylinder. *Journal of Fluid Mechanics* 22, 187–196.
- Gerrard, J.H., 1966. The mechanics of the formation region of vortices behind bluff bodies. *Journal of Fluid Mechanics* 25, 401–413.
- Graham, J.M.R., 1969. The effect of end plates on the two-dimensionality of a vortex wake. *The Aeronautical Quarterly* 20, 237–247.
- Lee, S.J., Lee, J.Y., 2006. Flow structure of wake behind a rotationally oscillating circular cylinder. *Journal of Fluids and Structures* 22, 1097–1112.

- Mahfouz, F.M., Badr, H.M., 2000. Flow structure in the wake of a rotationally oscillating cylinder. *ASME Journal of Fluids Engineering* 122, 290–301.
- Maskell, E.C., 1963. A theory of the blockage effects on bluff bodies and stalled wings in a closed wind tunnel. Aeronautical Research Council, Reports and Memoranda No. 3400.
- Ongoren, A., Rockwell, D., 1988. Flow structure from an oscillating cylinder: Part 1. Mechanisms of phase shift and recovery in the near wake. *Journal of Fluid Mechanics* 191, 197–223.
- Poncet, P., 2004. Topological aspects of three-dimensional wakes behind rotary oscillating cylinders. *Journal of Fluid Mechanics* 517, 27–53.
- Rae, W.H., Pope, A., 1984. *Low-speed Wind Tunnel Testing*, second ed. Wiley, New York.
- Shiels, D., Leonard, A., 2001. Investigation of a drag reduction on a circular cylinder in rotary oscillation. *Journal of Fluid Mechanics* 431, 297–322.
- Stansby, P.K., 1974. The effects of end plates on the base pressure coefficient of a circular cylinder. *Aeronautical Journal* 78, 36–37.
- Taneda, S., 1978. Visual observations of the flow past a circular cylinder performing a rotary oscillation. *Journal of the Physical Society of Japan* 45, 1038–1043.
- Tokumaru, P.T., Dimotakis, P.E., 1991. Rotary oscillation control of a cylinder wake. *Journal of Fluid Mechanics* 224, 77–90.
- West, G.S., Apelt, C.J., 1982. The effect of tunnel blockage and aspect ratio on the mean flow past a circular cylinder with Reynolds numbers between 10^4 and 10^5 . *Journal of Fluid Mechanics* 114, 361–377.
- Williamson, C.H.K., 1996. Vortex dynamics in the cylinder wake. *Annual Review of Fluid Mechanics* 28, 477–539.
- Williamson, C.H.K., Govardhan, R., 2004. Vortex-induced vibrations. *Annual Review of Fluid Mechanics* 36, 413–455.
- Zdravkovich, M.M., 1997. *Flow Around Circular Cylinders*, vol. 1. Oxford University Press, New York.